Research Article

For reprint orders, please contact: reprints@futuremedicine.com

Nanomedicine

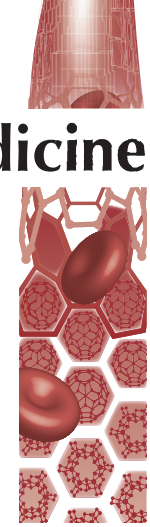

Poly(2-ethyl-2-oxazoline)–IR780 conjugate nanoparticles for breast cancer phototherapy

Cátia G Alves[1], Rita Lima-Sousa[1], Bruna L Melo[1], Paula Ferreira[2,3], André F Moreira[1], Ilídio J Correia*[,1,2] & Duarte de Melo-Diogo**[,1]

[1]CICS-UBI – Centro de Investigação em Ciências da Saúde, Universidade da Beira Interior, Avenida Infante D Henrique, Covilhã, 6200–506, Portugal

[2]CIEPQPF – Departamento de Engenharia Química, Universidade de Coimbra, Rua Sílvio Lima, Coimbra, 3030–790, Portugal

[3]Department of Chemical & Biological Engineering, Coimbra Institute of Engineering (ISEC), Rua Pedro Nunes, Coimbra, 3030–199, Portugal

*Author for correspondence: Tel.: +351 275 329 002; icorreia@ubi.pt

**Author for correspondence: demelodiogo@fcsaude.ubi.pt

Aims: To address the limitations of IR780 by preparing hydrophilic polymer–IR780 conjugates and to employ these conjugates in the assembly of nanoparticles (NPs) intended for cancer photothermal therapy. **Materials & methods:** The cyclohexenyl ring of IR780 was conjugated for the first time with thiol-terminated poly(2-ethyl-2-oxazoline) (PEtOx). This novel poly(2-ethyl-2-oxazoline)-IR780 (PEtOx-IR) conjugate was combined with D-α-tocopheryl succinate (TOS), leading to the assembly of mixed NPs (PEtOx-IR/TOS NPs). **Results:** PEtOx-IR/TOS NPs displayed optimal colloidal stability as well as cytocompatibility in healthy cells at doses within the therapeutic range. In turn, the combination of PEtOx-IR/TOS NPs and near-infrared light reduced heterotypic breast cancer spheroid viability to just 15%. **Conclusion:** PEtOx-IR/TOS NPs are promising agents for breast cancer photothermal therapy.

Plain language summary: Conventional anticancer approaches are often associated with severe side effects. Herein, the authors assembled a novel nanoparticle whose therapeutic effect is triggered by laser light. In *in vitro* assays, the produced nanomaterial was able to, after interacting with laser light, reduce the viability of classic and advanced cancer models. In these conditions, but in the absence of laser light, no cytotoxicity was observed. In this way, the on-demand effect (triggered by laser light) may contribute to reduced side effects. Moreover, the produced nanoparticle revealed good stability, which is important for its future translation.

Graphical abstract:

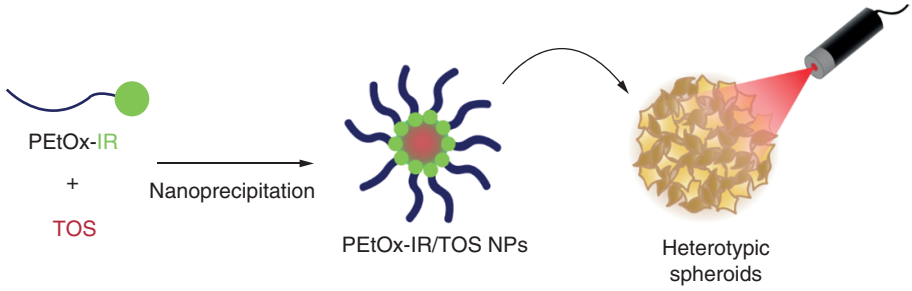

First draft submitted: 24 August 2022; Accepted for publication: 19 December 2022; Published online: 21 February 2023

Keywords: cancer • photothermal therapy • poly(2-ethyl-2-oxazoline) • polymer–IR780 conjugate • spheroids

Photoactivated materials have been showing promising results in cancer therapy [1,2]. This has been propelled by their ability to produce, upon interaction with light, a temperature increase (photothermal therapy [PTT]) and/or reactive oxygen species (photodynamic therapy [PDT]), which can damage cancer cells [3,4]. For these types of

Future Medicine

applications, it is of extreme importance to use the first window of near-infrared (NIR; 750–1000 nm) light because of its suitable penetration depth and minimal interactions with biological components (e.g., collagen, melanin and water), thus ensuring minimal off-target effects [4,5].

Owing to these reasons, the use of NIR light-absorbing agents is crucial in cancer PTT/PDT. In this context, US FDA approval of indocyanine green for angiography as well as its NIR absorption has driven investigations into its use for cancer phototherapy [6,7]. However, the shortcomings of indocyanine green (e.g., low fluorescence quantum yield and photodegradability) have motivated the development of other heptamethine cyanines [4,8]. The properties of different NIR light-absorbing prototypic heptamethine cyanines were recently analyzed and it was disclosed that IR780 holds great potential, as a result of its high NIR absorption, strong photothermal/photodynamic capabilities and applicability for cancer cell imaging [4]. Nevertheless, the direct use of IR780 for cancer PTT/PDT is limited by its low water solubility and cytotoxic profile [9].

The limitations of IR780 can be overcome through the conjugation of its cyclohexenyl ring with hydrophilic polymers [10–12]. In fact, preparation of hydrophilic polymer–IR780 conjugates leads to improved solubility and cytocompatibility [10,13]. Moreover, the amphiphilic nature of these hydrophilic polymer–IR780 conjugates enables their assembly into nanostructures [10,11]. This rearrangement of polymer–IR780 conjugate linear chains into nanosized materials is of paramount importance because of the capacity of nanostructures with well-defined physicochemical properties to accumulate at the tumor site after intravenous administration [10,14]. Moreover, the use of nanomaterials assembled using polymer–drug conjugates is often associated with a more controlled release profile and higher drug loading capacity compared with the direct loading of drugs into the hydrophobic core of nanomaterials [15–17].

In this study, a novel polymer–IR780 conjugate was prepared by attaching thiol-terminated poly(2-ethyl-2-oxazoline) (PEtOx) to the cyclohexenyl ring of IR780. PEtOx was selected because of its biocompatibility and capacity to reduce protein adsorption on the surface of nanomaterials, hence improving blood circulation time and tumor uptake [18–23]. PEtOx was also chosen as an alternative to PEG since several reports have highlighted that PEGylated nanomaterials can be immunogenic [24–26]. The poly(2-ethyl-2-oxazoline)-IR780 (PEtOx-IR) conjugates were then combined with D-α-tocopheryl succinate (TOS) because of the ability of the latter to facilitate the assembly of nanoparticles (NPs) by stabilizing the nanostructure core [27].

Materials & methods

Materials

IR780 iodide, poly(2-ethyl-2-oxazoline) α-benzyl ω-thiol terminated (PEtOx-SH; M_n = 10,000 Da), TOS, resazurin, paraformaldehyde, DMEM-F12 and trypsin were acquired from Sigma-Aldrich (Sintra, Portugal). Acetone, chloroform, Triton X-100 and methanol were purchased from Thermo Fisher Scientific (Oeiras, Portugal). Agarose was purchased from GRiSP (Porto, Portugal). The Michigan Cancer Foundation-7 (MCF-7) cell line was acquired from American Type Culture Collection (Middlesex, UK), and normal human dermal fibroblasts (NHDFs) were obtained from PromoCell (Heidelberg, Germany). Triethylamine was purchased from TCI (Oxford, UK). Cell imaging plates were obtained from ibidi GmbH (Munich, Germany). Calcein AM, Hoechst 33342®, propidium iodide (PI), cell culture plates and T-flasks were purchased from Thermo Fisher Scientific (Porto, Portugal). Fetal bovine serum (FBS) was obtained from Biochrom AG (Berlin, Germany). Water used in all experiments was double-deionized (0.22-µm filter, 18.2 M Ω cm).

PEtOx-IR conjugate synthesis & characterization

Synthesis of the PEtOx-IR conjugate was performed by adapting protocols described elsewhere [13,28]. Initially, IR780 (66.7 mg) and PEtOx-SH (40 mg) were dissolved in chloroform (50 ml) containing triethylamine (50 µl). A molar excess of IR780 to the available thiol-groups of PEtOx-SH was used. The solution was stirred for 48 h at room temperature. Next, the chloroform was removed by evaporation (Rotavapor® R-215; Büchi, Flawil, Switzerland) and the obtained product was resuspended in methanol. Subsequently, dialysis against methanol was performed (1-kDa molecular weight cutoff membrane) for 24 h to remove the nonconjugated IR780. After this process, the obtained methanolic solution containing the PEtOx-IR conjugate was concentrated by evaporation and stored at 4°C.

Synthesis of the PEtOx-IR conjugate was confirmed by FTIR spectroscopy (Nicolet iS10 spectrometer; Thermo Fisher Scientific, MA, USA) and proton nuclear magnetic resonance (^{1}H NMR) (Avance III 400-MHz spectrometer; Bruker, NY, USA). For ^{1}H NMR analysis, IR780, PEtOx-SH and PEtOx-IR conjugate were dissolved in deuterated

chloroform. To analyze the ^{1}H NMR spectra, the authors used MNova software (Mestrelab Research, SL, Santiago de Compostela, Spain).

Formulation of PEtOx-IR/TOS & PEtOx-IR NPs

The nanoprecipitation technique was used to formulate PEtOx-IR/TOS NPs by adapting a previously described protocol [29]. First, 1 ml of acetone containing 0.5 mg of PEtOx-IR conjugate and 0.5 mg of TOS was added dropwise to 5 ml of phosphate-buffered saline (PBS) under constant stirring for 2 h at room temperature. Afterward, the solution was recovered, dialyzed against water (0.5- to 1-kDa molecular weight cutoff membrane) for 90 min at room temperature and filtered (0.45-µm pore size), yielding PEtOx-IR/TOS NPs. The same protocol was used to prepare PEtOx-IR NPs (i.e., particles without TOS). In this case, only PEtOx-IR conjugate (0.5 mg) was added to the acetone solution and the filtration step was not performed.

NP physicochemical, optical & photothermal characterization

Dynamic light scattering was used to evaluate the size distribution of PEtOx-IR/TOS and PEtOx-IR NPs (Zetasizer Nano ZS; Malvern Panalytical Ltd, Malvern, UK) in water. The zeta potential of PEtOx-IR/TOS NPs in DMEM-F12 medium supplemented with 10% (v/v) FBS was also determined. The morphology of PEtOx-IR/TOS NPs was characterized by transmission electron microscopy (Tecnai G^2 20 S-TWIN; FEI Europe BV, Eindhoven, The Netherlands) operated at an accelerating voltage of 200 kV. For this analysis, NPs were first stained with 2% (w/v) of phosphotungstic acid.

The incorporation efficiency of the PEtOx-IR conjugate in PEtOx-IR/TOS NPs was determined by UV-VIS-NIR absorption spectroscopy. First, a standard curve of the PEtOx-IR conjugate in 1:1 (v/v) water:methanol was performed at 780 nm using an Evolution 201 spectrophotometer (Thermo Fisher Scientific). Next, PEtOx-IR/TOS NPs were freeze-dried in a ScanVac CoolSafe (LaboGene ApS, Lynge, Denmark) and resuspended in 1:1 (v/v) water:methanol. The concentration of PEtOx-IR conjugate was then determined by analyzing the absorbance of the freeze-dried PEtOx-IR/TOS NP solution at 780 nm. Finally, the incorporation efficiency was determined according to the following equation:

$$\textit{Incorporation Efficiency}\ (\%) = \frac{\textit{Weight of PEtOxIR conjugate incorporated in PEtOxIR/TOS NPs}}{\textit{Weight of PEtOxIR conjugate initially fed}} \times 100$$

To evaluate the capacity of PEtOx-IR/TOS NPs to interact with NIR light, their VIS-NIR absorption spectrum was acquired. To this end, the authors analyzed the absorption of PEtOx-IR/TOS NPs at 5 µg ml^{-1} PEtOx-IR conjugate equivalents in water and PEtOx-IR conjugate at 5 µg ml^{-1} in methanol. To evaluate the colloidal stability of PEtOx-IR/TOS NPs, the authors investigated their size variation and VIS-NIR absorption spectrum when dispersed in water, PBS and cell culture medium consisting of DMEM-F12 supplemented with 10% (v/v) FBS for 48 h.

Finally, the photothermal capacity of PEtOx-IR/TOS NPs was evaluated by determining the temperature variations attained upon NIR laser irradiation (808 nm; 1.7 W.cm^{-2}; 5 min) using a thermocouple thermometer [30]. Irradiated water was used as a control. To assess the photostability of PEtOx-IR/TOS NPs, the authors acquired their VIS-NIR absorption spectrum after each minute of NIR irradiation. Furthermore, the authors evaluated the temperature variations induced by PEtOx-IR/TOS NPs at 20 µg ml^{-1} of PEtOx-IR conjugate equivalents, measured at the fifth minute of NIR laser exposure along five cycles of irradiation. A new irradiation cycle was only started after complete cooling of the formulation to room temperature.

Cytocompatibility of PEtOx-IR/TOS & PEtOx-IR NPs in 2D *in vitro* cultures

The cytocompatibility of PEtOx-IR/TOS and PEtOx-IR NPs in 2D *in vitro* cell cultures was evaluated using the resazurin method [31]. For this assay, MCF-7 (breast cancer cell models) and NHDF (normal cell models) cells were seeded in 96-well plates at a density of 1 × 10^4 cells/well. Both cell lines were cultured in DMEM-F12 medium supplemented with 10% (v/v) FBS and 1% (v/v) streptomycin/gentamicin in a humidified incubator at 37°C and 5% CO_2. After 24 h, the culture medium was replaced with fresh medium containing different concentrations of PEtOx-IR/TOS NPs or PEtOx-IR NPs. After 24 and 48 h, the medium was then removed and fresh culture medium with 10% (v/v) resazurin was incubated for 4 h in the dark at 37°C and 5% CO_2. Finally, to evaluate cell viability, the fluorescence of resorufin ($\lambda_{ex}/\lambda_{em}$ = 560/590 nm) was measured in a SpectraMax Gemini EM

spectrofluorometer (Molecular Devices LLC, CA, USA). Cells incubated solely with medium or 70% (v/v) ethanol were used as negative and positive controls, respectively.

Cellular uptake of PEtOx-IR/TOS NPs in 2D *in vitro* cancer models

Prior to evaluating the cellular uptake of PEtOx-IR/TOS NPs, the fluorescence emitted by this formulation was assessed in a spectrofluorometer (λ_{ex} = 633 and 780 nm). To evaluate the uptake of PEtOx-IR/TOS NPs by MCF-7 cells, 1×10^4 cells/well were seeded in 96-well plates. After 24 h, the cells were incubated with fresh medium containing PEtOx-IR/TOS NPs at 2.5 μg ml^{-1} of PEtOx-IR conjugate equivalents or IR780 at 2.5 μg ml^{-1}. After 4 h, noninternalized NPs were removed by washing cells with ice-cold Krebs–Ringer buffer. Afterward, cells were incubated for 30 min with 1% (v/v) Triton X-100 in Krebs–Ringer buffer to cause their lysis. To determine PEtOx-IR/TOS NP uptake, the fluorescence of PEtOx-IR conjugate present in the cell lysate was analyzed with a spectrofluorometer ($\lambda_{ex}/\lambda_{em}$ = 780/800 nm). Cells incubated with only Krebs–Ringer buffer were used as a control.

To further observe the uptake of PEtOx-IR/TOS NPs, confocal laser scanning microscopy (CLSM) images were acquired using an LSM 710 confocal microscope (Carl Zeiss AG, Oberkochen, Germany). To this end, MCF-7 cells were seeded at 1.5×10^4 cells/well in μ-Slide eight-well imaging plates (ibidi GmbH). Two days later, the medium was replaced with fresh medium containing PEtOx-IR/TOS NPs at 5 μg ml^{-1} of PEtOx-IR conjugate equivalents. After 4 h, the medium was removed and several washing steps were performed with PBS. Paraformaldehyde 4% was used to fix cells for 15 min at room temperature and Hoescht 33342® was used to label the cell nucleus for 45 min at 4°C. Fluorescence images were acquired using $\lambda_{ex}/\lambda_{em}$ of 633/656–758 nm to visualize IR780 and 405/410–499 nm to visualize Hoechst 33342®.

Phototherapeutic effect mediated by PEtOx-IR/TOS NPs in 2D *in vitro* cancer models

The phototherapeutic effect of PEtOx-IR/TOS NPs in 2D *in vitro* cancer models was evaluated as previously reported [29]. First, MCF-7 cells were seeded as described earlier. After 24 h, the culture medium was replaced with fresh medium containing PEtOx-IR/TOS NPs at 2.5 and 5 μg ml^{-1} of PEtOx-IR conjugate equivalents. After 4 h, the cells were exposed to NIR irradiation (808 nm; 1.7 W.cm^{-2}; 5 min). After reaching a total of 24 h of incubation with the nanomaterials, cell viability was measured using resorufin fluorescence as described earlier.

CLSM images were also acquired to visualize the phototherapeutic effect of PEtOx-IR/TOS NPs. MCF-7 cells were seeded in μ-Slide eight-well imaging plates as described earlier. Next, cells were incubated with fresh medium containing PEtOx-IR/TOS NPs at 2.5 and 5 μg ml^{-1} of PEtOx-IR conjugate equivalents. After 4 h, cells were irradiated with NIR light (808 nm; 1.7 W.cm^{-2}; 5 min). The medium was then removed, and live and dead cells were stained with calcein AM and PI, respectively, for 15 min according to the manufacturer's protocol. Fluorescence images were acquired using $\lambda_{ex}/\lambda_{em}$ of 488/493–556 nm to visualize calcein AM and 561/566–719 nm to visualize PI. Cells incubated solely with culture medium were used as the control for live cells.

Penetration capacity of PEtOx-IR/TOS NPs in 3D *in vitro* cancer models

Heterotypic breast cancer spheroids were produced as previously described [9,30]. In brief, 2% (w/v) agarose structures with round-bottom microwells were produced using a micromold (3D Petri Dish; MicroTissues Inc., RI, US). Next, 1×10^6 MCF-7 and NHDF cells, at a ratio of 1:1, were seeded per structure, forming 81 spheroids per agarose construct. Every 2 days, the medium was replaced with fresh DMEM-F12 medium supplemented with 10% (v/v) FBS and 1% (v/v) streptomycin/gentamicin. Spheroids were left to grow for 10 days in an incubator with a humidified atmosphere at 37°C and 5% CO_2.

To visualize the penetration of NPs into the spheroids, they were incubated with fresh medium containing PEtOx-IR/TOS NPs at 7.5 μg ml^{-1} of PEtOx-IR conjugate equivalents. After 24 h, spheroids were fixed with paraformaldehyde 4% overnight and NP penetration capacity was visualized by CLSM using $\lambda_{ex}/\lambda_{em}$ of 633/656–758 nm to visualize IR780. Fluorescence intensity plots across the diameter of the spheroid were determined at different z-stacks using ImageJ software as previously described [30].

Phototherapeutic effect mediated by PEtOx-IR/TOS NPs in 3D *in vitro* cancer models

To evaluate the phototherapeutic capacity of PEtOx-IR/TOS NPs in 3D *in vitro* cancer models, spheroids were produced and maintained as described earlier. After growing for 10 days, PEtOx-IR/TOS NPs (7.5 and 15 μg ml^{-1} of PEtOx-IR conjugate equivalents) were incubated in fresh medium in the spheroids for 24 h. Next, spheroids

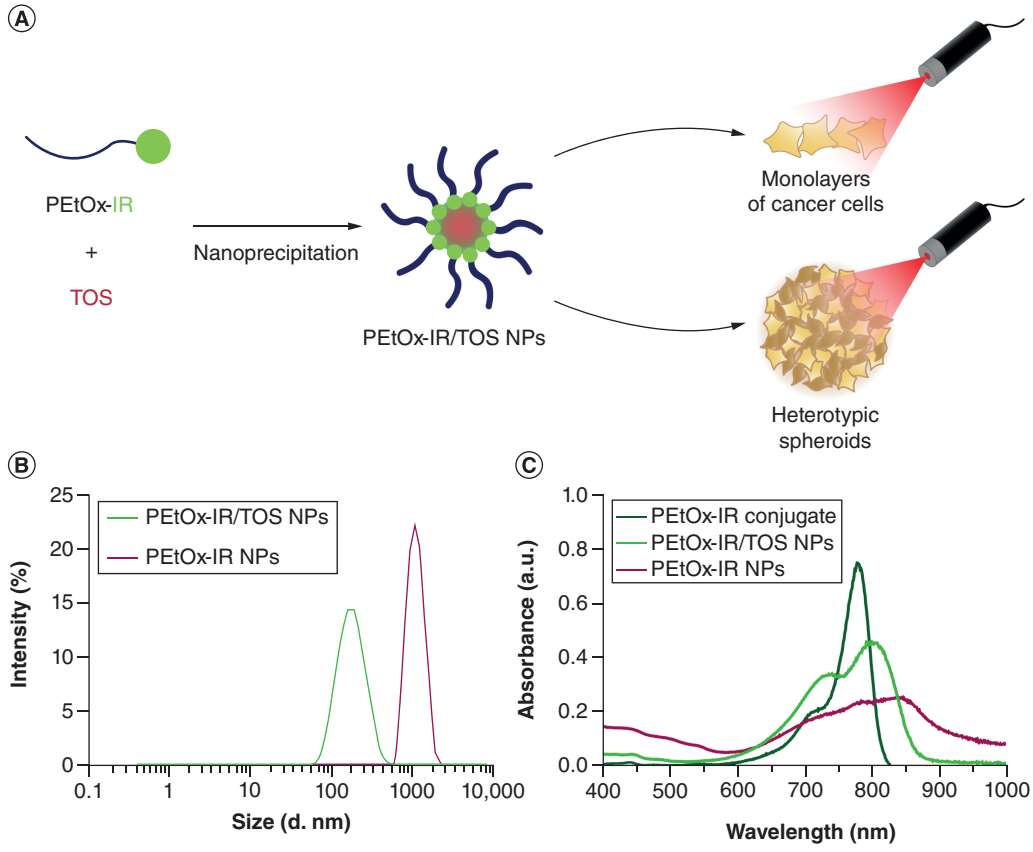

Figure 1. Formulation and characterization of poly(2-ethyl-2-oxazoline)–IR780/D-α-tocopheryl succinate nanoparticles. (A) Schematic representation of NP formulation and application in cancer phototherapy. **(B)** Dynamic light scattering size distribution of PEtOx-IR/TOS and PEtOx-IR NPs. **(C)** VIS–near-infrared spectra of PEtOx-IR conjugate in methanol at 5 μg ml^{-1} and PEtOx-IR/TOS and PEtOx-IR NPs in water at 5 μg ml^{-1} of PEtOx-IR conjugate equivalents.
NP: Nanoparticle; PEtOx-IR: Poly(2-ethyl-2-oxazoline)–IR780; TOS: D-α-tocopheryl succinate.

were irradiated with NIR light (808 nm; 1.7 W.cm^{-2}; 5 min). After 48 h, spheroid viability was evaluated using the resazurin method as described earlier. Each experimental condition was evaluated in 30 spheroids.

To visualize the phototherapeutic effect in spheroids, they were incubated with PEtOx-IR/TOS NPs at 15 μg ml^{-1} of PEtOx-IR conjugate equivalents. After 24 h, spheroids were irradiated with NIR light (808 nm; 1.7 W.cm^{-2};5 min). Finally, calcein AM/PI was used to stain the spheroids. Fluorescence images were acquired as described earlier. Spheroids incubated solely with culture medium were used as the control for nontreated spheroids.

Statistical analysis

To compare the multiple groups, the authors used one-way analysis of variance with Student–Newman–Keuls test. Statistical analysis of two groups was performed using the unpaired Student's *t* test. The trial version of Prism 6.0 (GraphPad Software, CA, USA) was used to perform data analysis. $p < 0.05$ was considered statistically significant.

Results

Formulation & characterization of PEtOx-IR/TOS NPs

Initially, the PEtOx-IR conjugate was synthesized by binding the cyclohexenyl ring of IR780 with the thiol group of PEtOx-SH [13]. FTIR spectroscopy and ^{1}H NMR data of the PEtOx-IR conjugate are discussed in Supplementary Figures 1 & 2. Next, the PEtOx-IR conjugate was used to produce PEtOx-IR NPs through a simple nanoprecipitation technique (Figure 1A). The dynamic light scattering data revealed that PEtOx-IR NPs had sizes between 712 and 1990 nm, with an average size of 1092.0 ± 197.9 nm and polydispersity index of 0.293 (batch triplicates) (Figure 1B).

10.2217/nnm-2022-0218

To improve the formulation's size distribution, TOS was included in the nanoprecipitation technique, as TOS can stabilize the nanomaterial core [27]. PEtOx-IR/TOS NPs demonstrated a size of 189.7 ± 4.4 nm (batch triplicates) as well as a low polydispersity index of 0.164 (Figure 1B). PEtOx-IR/TOS NPs were then imaged by transmission electron microscopy and revealed a spherical shape (Supplementary Figure 3). Moreover, PEtOx-IR/TOS NPs showed a zeta potential of -7.8 ± 0.9 mV. The incorporation efficiency of the PEtOx-IR conjugate in PEtOx-IR/TOS NPs was 39 ± 3% (n = 5).

Next, the colloidal stability of PEtOx-IR/TOS NPs was evaluated by dispersing them in water, PBS and cell culture medium consisting of DMEM-F12 supplemented with 10% (v/v) FBS. The size and NIR absorption of PEtOx-IR/TOS NPs did not demonstrate any meaningful variation over time (Supplementary Figure 4). By contrast, the NIR absorption of PEtOx-IR NPs decreased over time (Supplementary Figure 5). This phenomenon was also accompanied by evident changes in the color of the PEtOx-IR NPs solution (Supplementary Figure 6).

To assess the ability of PEtOx-IR/TOS NPs to interact with NIR light, the authors acquired their absorption spectrum (Figure 1C). Compared with the PEtOx-IR conjugate, the absorption of PEtOx-IR/TOS NPs had a red shift. Because of this, PEtOx-IR/TOS NPs had a 2.74-fold higher absorption at 808 nm compared with the PEtOx-IR conjugate. Interestingly, PEtOx-IR NPs had a 1.89-fold weaker absorption at this wavelength compared with PEtOx-IR/TOS NPs.

Finally, the photothermal capacity of PEtOx-IR/TOS NPs was evaluated by recording the temperature changes mediated by this nanoformulation during NIR irradiation (808 nm; 1.7 $W.cm^{-2}$; 5 min) (Supplementary Figure 7A). PEtOx-IR/TOS NPs produced a concentration-dependent photoinduced heat, achieving the maximum temperature increase after 1–2 min of irradiation. At a concentration of 20 μg ml^{-1} of PEtOx-IR conjugate equivalents, PEtOx-IR/TOS NPs produced a temperature increase of 12.5°C after 2 min of exposure to NIR light [4,32]. Moreover, the response of water (control) to NIR light was not meaningful ($\Delta T < 1.4$°C) (Supplementary Figure 7A).

Evaluation of PEtOx-IR/TOS NP cytocompatibility in 2D *in vitro* cultures

Subsequently, the authors evaluated the cytocompatibility of PEtOx-IR and PEtOx-IR/TOS NPs in 2D *in vitro* cultures of NHDF (normal cell line) and MCF-7 (breast cancer cell line) cells (Figure 2). NHDFs exposed to PEtOx-IR NPs for 24 and 48 h displayed greater than 76% viability (Figure 2A). MCF-7 cells incubated with PEtOx-IR NPs at up to 5 μg ml^{-1} of PEtOx-IR conjugate equivalents also remained highly viable (Figure 2B). For higher doses of PEtOx-IR NPs (7.5 and 10 μg ml^{-1} of PEtOx-IR conjugate equivalents), the viability of MCF-7 cells was impaired.

NHDF and MCF-7 cells incubated with PEtOx-IR/TOS NPs for 24 h at up to 5 μg ml^{-1} of PEtOx-IR conjugate equivalents demonstrated a viability of 82 and 80%, respectively (Figure 2C & D). An incubation period of 48 h with this same dose of PEtOx-IR/TOS NPs revealed similar viability in NHDFs (83%) and a small decrease in MCF-7 cell viability to 65%. However, incubation of both cell lines with greater doses of PEtOx-IR/TOS NPs (7.5 and 10 μg ml^{-1} of PEtOx-IR conjugate equivalents) led to high cytotoxicity.

Determination of ability of PEtOx-IR/TOS NPs to be internalized in cancer cells & phototherapeutic capacity

The authors investigated the capacity of PEtOx-IR/TOS NPs to be internalized by monolayers of cancer cells in 2D *in vitro* cancer cell models (Figure 3). To this end, the authors analyzed the fluorescence emitted by PEtOx-IR/TOS NPs deriving from the IR780 molecule present on the PEtOx-IR conjugate (Figure 3 & Supplementary Figure 8A). CLSM images revealed that MCF-7 cells incubated with PEtOx-IR/TOS NPs had IR780 fluorescence signals in the cytoplasm (Figure 3). This result was further confirmed by analyzing the IR780 fluorescence intensity in MCF-7 cells incubated with PEtOx-IR/TOS NPs (Supplementary Figure 8B & C).

After confirming the ability of PEtOx-IR/TOS NPs to be internalized by cancer cells, their phototherapeutic capacity was determined (Figure 4A). In line with the previous observations, MCF-7 cells exposed solely to NIR light or nonirradiated PEtOx-IR/TOS NPs remained highly viable (>80%) (Figure 4B). By contrast, the combination of NIR light and PEtOx-IR/TOS NPs, at 2.5 μg ml^{-1} of PEtOx-IR conjugate equivalents, reduced MCF-7 cell viability to 20%. By further increasing the concentration to 5 μg ml^{-1} of PEtOx-IR conjugate equivalents, the photothermal heating induced by PEtOx-IR/TOS NPs reduced cancer cell viability to just 9%. These results were also confirmed by imaging MCF-7 cells stained with calcein AM (labels live cells) and PI (labels dead cells) after the different treatments (Figure 4C & D). As expected, the CLSM images revealed calcein AM fluorescence in the

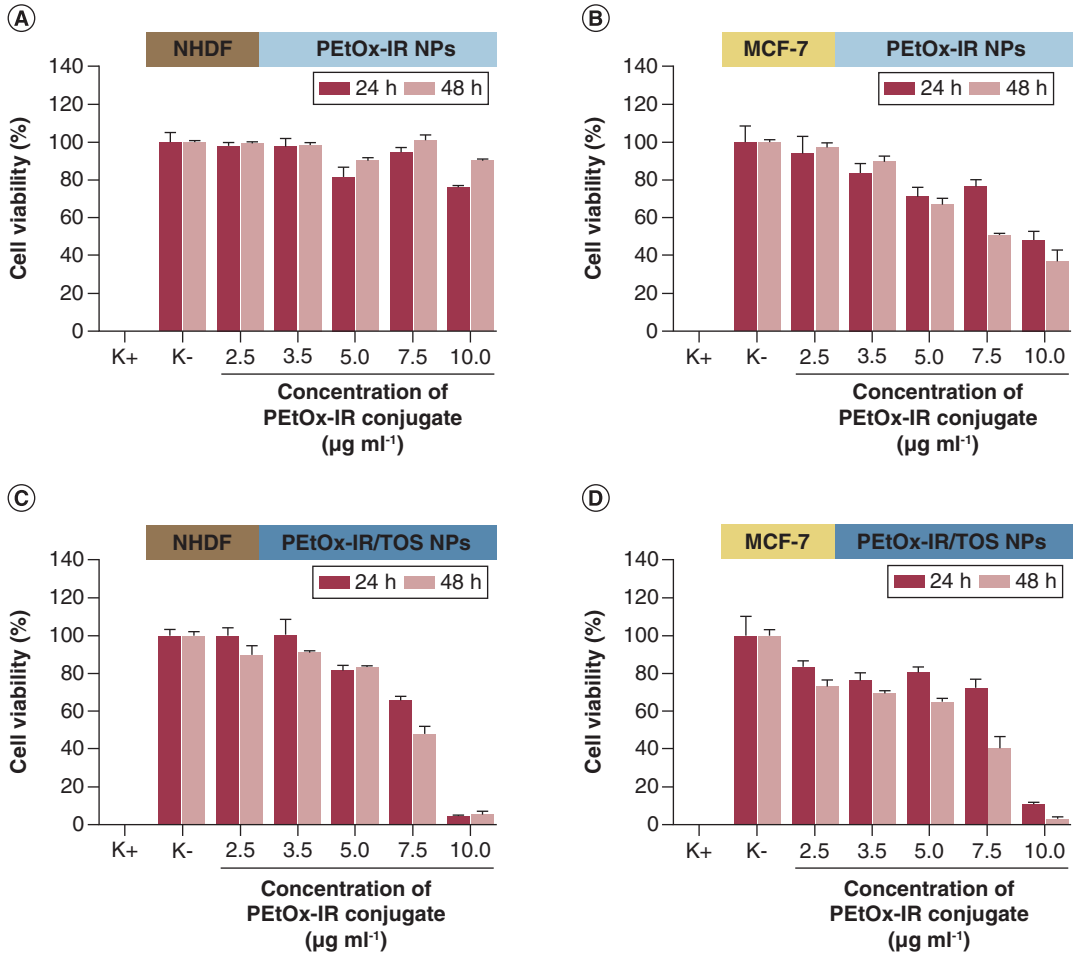

Figure 2. Cytocompatibility of poly(2-ethyl-2-oxazoline)–IR780 and poly(2-ethyl-2-oxazoline)–IR780/D-α-tocopheryl succinate nanoparticles. Cell viability of **(A)** NHDF and **(B)** MCF-7 cells after incubation with PEtOx-IR NPs at different concentrations of PEtOx-IR conjugate equivalents for 24 and 48 h. Cell viability of **(C)** NHDF and **(D)** MCF-7 cells after incubation with PEtOx-IR/TOS NPs at different concentrations of PEtOx-IR conjugate equivalents for 24 and 48 h. Positive control (K+) was cells treated with 70% (v/v) ethanol and negative control (K-) was cells incubated with only cell culture medium. Data are presented as mean ± standard deviation (n = 5).
MCF-7: Michigan Cancer Foundation-7; NHDF: Normal human dermal fibroblast; NP: Nanoparticle; PEtOx-IR: Poly(2-ethyl-2-oxazoline)–IR780; TOS: D-α-tocopheryl succinate.

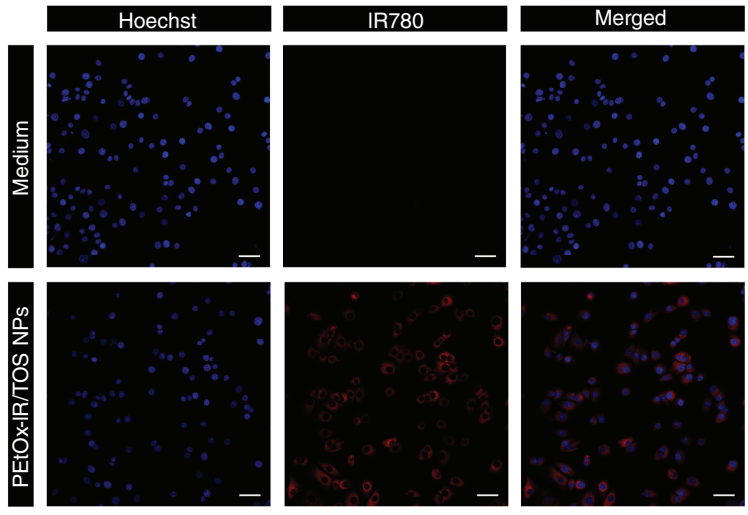

Figure 3. Uptake of poly(2-ethyl-2-oxazoline)–IR780/D-α-tocopheryl succinate nanoparticles at 5 μg ml^{-1} of poly(2-ethyl-2-oxazoline)–IR780 conjugate equivalents by Michigan Cancer Foundation-7 cells. Blue channel = Hoechst 33342®-stained nucleus. Red channel = IR780. Scale bar = 50 μm.
NP: Nanoparticle; PEtOx-IR: Poly(2-ethyl-2-oxazoline)–IR780; TOS: D-α-tocopheryl succinate.

10.2217/nnm-2022-0218

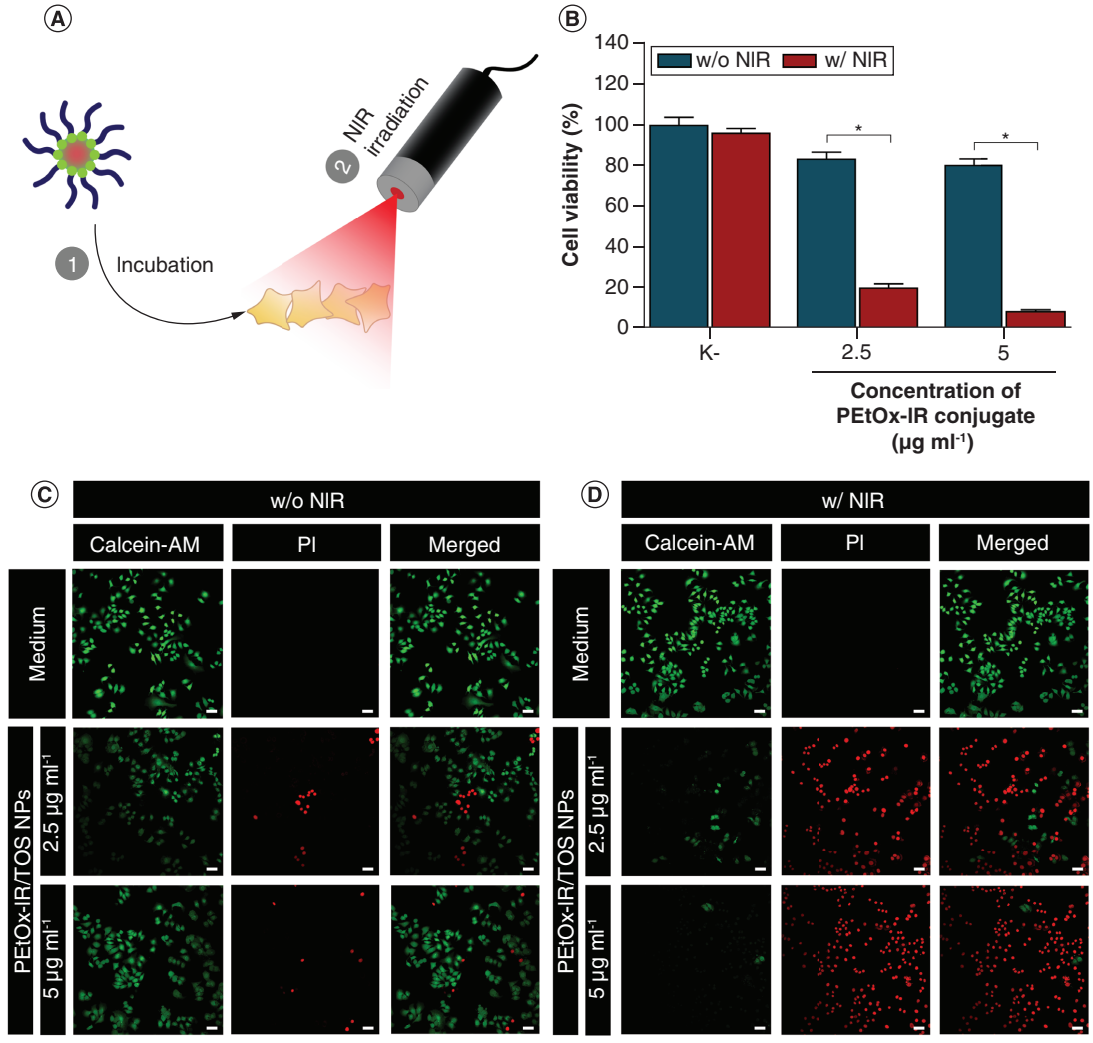

Figure 4. Phototherapeutic effect of poly(2-ethyl-2-oxazoline)–IR780/D-α-tocopheryl succinate nanoparticles in 2D *in vitro* cancer cell models. (A) Schematic representation of therapeutic procedure. **(B)** Evaluation of the effect of PEtOx-IR/TOS NPs at different concentrations of PEtOx-IR conjugate equivalents w/o NIR and w/ NIR laser irradiation (808 nm; 1.7 W.cm^{-2}; 5 min) on viability of Michigan Cancer Foundation-7 cells. K- w/o NIR (negative control) represents cells incubated only with culture medium and K- w/ NIR represents cells exposed solely to NIR light. Data are presented as mean ± standard deviation (n = 5). Confocal laser scanning microscopy images of Michigan Cancer Foundation-7 cells stained with calcein AM/PI after exposure to PEtOx-IR/TOS NPs **(C)** w/o NIR or **(D)** w/ NIR laser irradiation. Medium w/o NIR represents the control for live cells and medium w/ NIR represents cells exposed solely to NIR light. Green channel = calcein AM. Red channel = PI. Scale bar = 50 μm.
*$p < 0.0001$.
NIR: Near-infrared; NP: Nanoparticle; PEtOx-IR: Poly(2-ethyl-2-oxazoline)–IR780; PI: Propidium iodide; TOS: D-α-tocopheryl succinate; w/: With; w/o: Without.

vast majority of cancer cells exposed to only NIR light or nonirradiated PEtOx-IR/TOS NPs, whereas cancer cells were almost exclusively stained with PI upon exposure to PEtOx-IR/TOS NPs plus NIR light.

Evaluation of PEtOx-IR/TOS NP penetration & phototherapeutic effect in heterotypic spheroids

The authors then investigated the ability of PEtOx-IR/TOS NPs to penetrate into spheroids in 3D *in vitro* cancer models (Figure 5A). To this end, spheroids were incubated with PEtOx-IR/TOS NPs, and the authors acquired CLSM images at different z-stacks as well as the respective fluorescence intensity plots. Fluorescence signals could be observed in the spheroids, indicating the ability of PEtOx-IR/TOS NPs to penetrate into these 3D cellular aggregates. A closer inspection revealed that the fluorescence was mostly located at the spheroids' periphery.

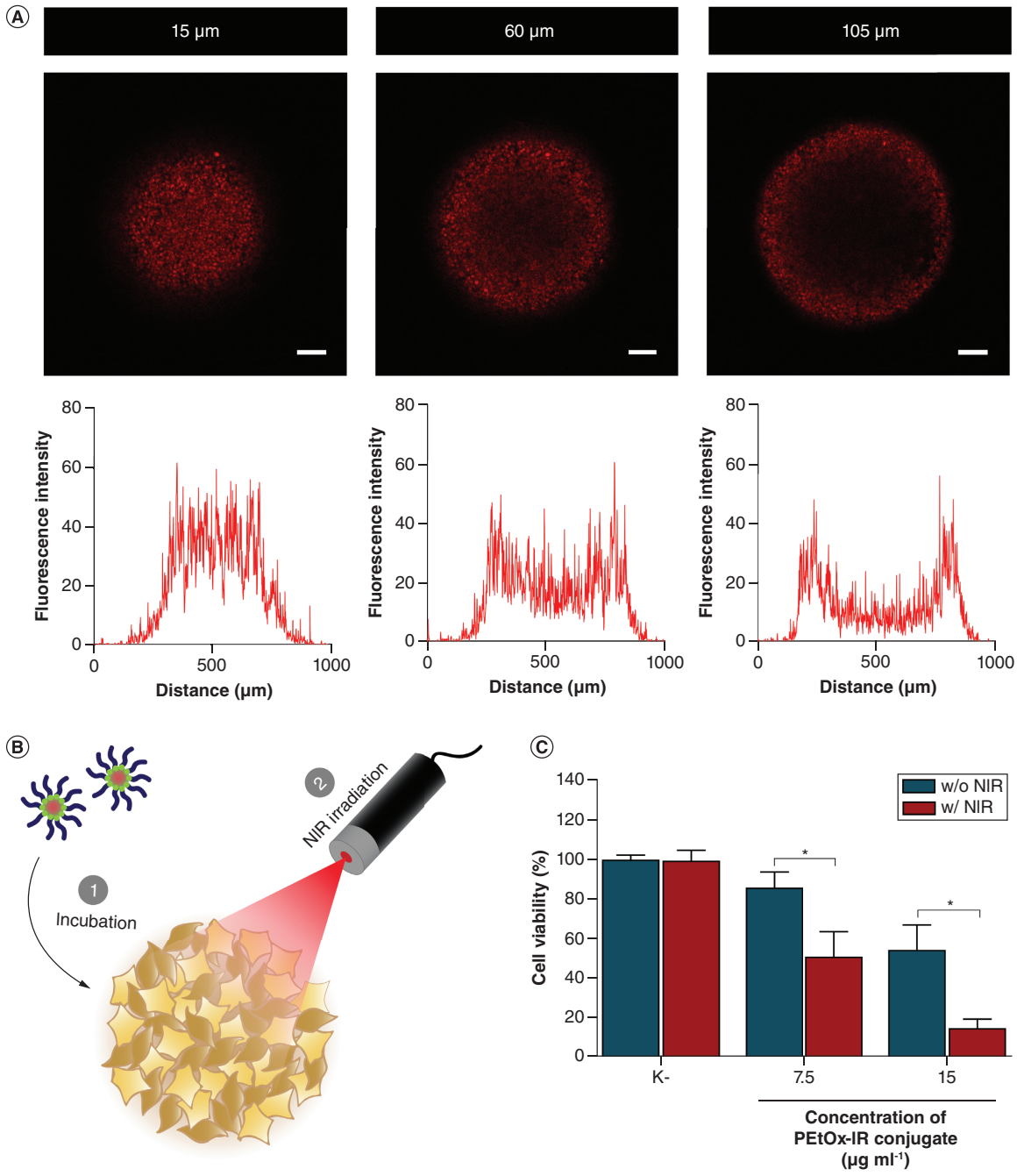

Figure 5. Phototherapeutic effect of poly(2-ethyl-2-oxazoline)–IR780/D-α-tocopheryl succinate nanoparticles in 3D *in vitro* cancer models. (A) Confocal laser scanning microscopy z-stacks of spheroids after incubation with PEtOx-IR/D-α-tocopheryl succinate nanoparticles at 7.5 µg ml^{-1} of PEtOx-IR conjugate equivalents, at different penetration depths and respective fluorescence intensity plots across the diameter of spheroids. Red channel = IR780. Scale bar = 100 µm. **(B)** Schematic representation of therapeutic procedure in heterotypic spheroids. **(C)** Evaluation of effect of PEtOx-IR/D-α-tocopheryl succinate nanoparticles at different concentrations of PEtOx-IR conjugate equivalents w/o NIR and w/ NIR laser irradiation (808 nm; 1.7 W.cm^{-2}; 5 min) on the viability of spheroids. K- w/o NIR (negative control) represents spheroids incubated only with culture medium and K- w/ NIR represents spheroids exposed solely to NIR light. Data are presented as mean ± standard deviation (n = 30).
*$p < 0.0001$.
NIR: Near-infrared; PEtOx-IR: Poly(2-ethyl-2-oxazoline)–IR780; w/: With; w/o: Without.

10.2217/nnm-2022-0218

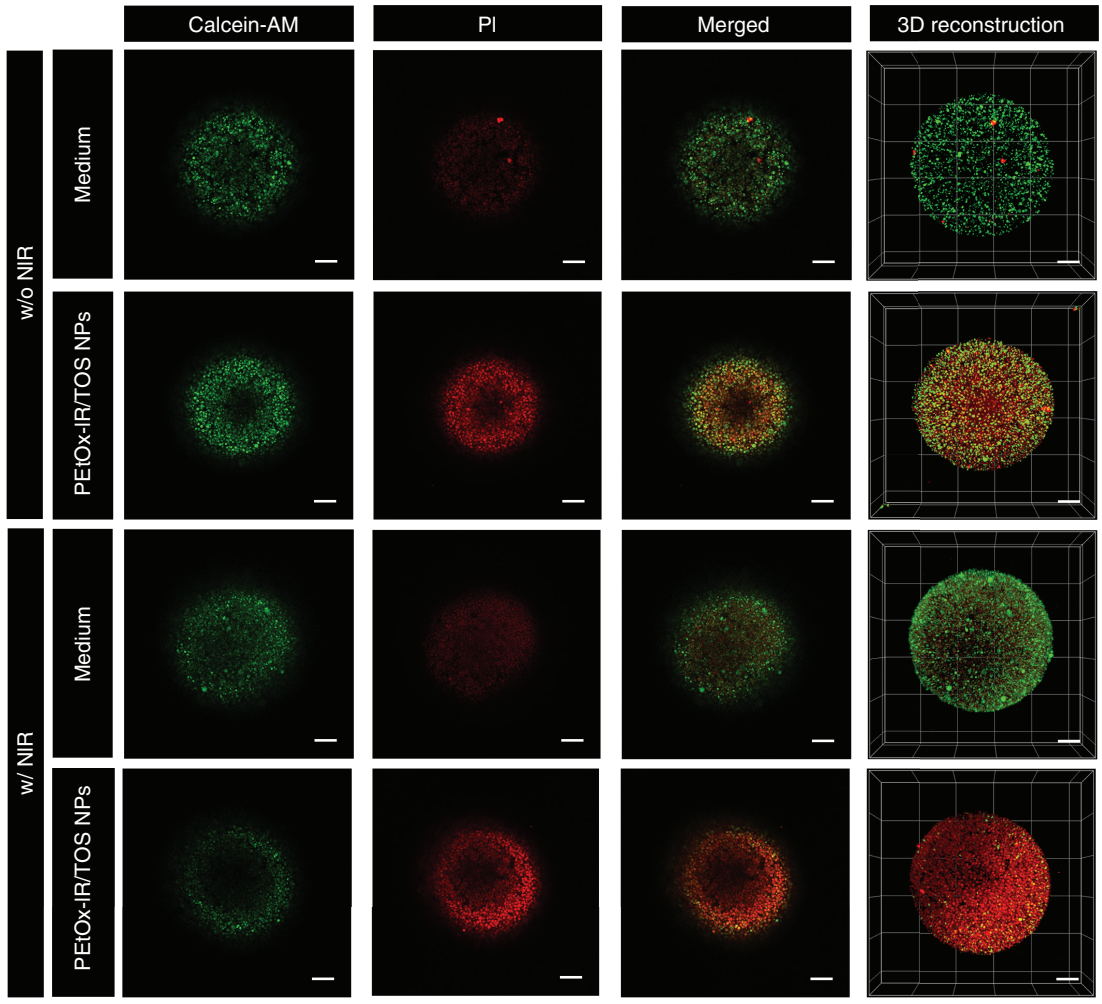

Figure 6. Live/dead analysis of spheroids. Confocal laser scanning microscopy images of spheroids stained with calcein AM/PI after exposure to PEtOx-IR/TOS NPs at 15 μg ml^{-1} of PEtOx-IR conjugate equivalents w/o NIR or w/ NIR irradiation (808 nm; 1.7 $W.cm^{-2}$; 5 min). Medium w/o NIR represents nontreated spheroids and medium w/ NIR represents spheroids exposed solely to NIR irradiation. Green channel = calcein AM. Red channel = PI. Scale bar = 100 μm.
NIR: Near-infrared; NP: Nanoparticle; PEtOx-IR: Poly(2-ethyl-2-oxazoline)–IR780; PI: Propidium iodide; TOS: D-α-tocopheryl succinate; w/: With; w/o: Without.

Finally, the authors investigated the phototherapeutic capacity of PEtOx-IR/TOS NPs in the spheroids (Figure 5B). As expected, NIR irradiation per se did not affect spheroid viability (Figure 5C). Considering the greater resistance of spheroids to therapeutic action [33,34], they were incubated with a higher dose of PEtOx-IR/TOS NPs compared with the cancer cell monolayers. Spheroids exposed to PEtOx-IR/TOS NPs at 7.5 μg ml^{-1} of PEtOx-IR conjugate equivalents displayed a viability of 86% (Figure 5C). At the same dose, the combination of PEtOx-IR/TOS NPs and NIR light further decreased spheroid viability to 51%. Moreover, the phototherapeutic effect mediated by PEtOx-IR/TOS NPs at 15 μg ml^{-1} of PEtOx-IR conjugate equivalents reduced spheroid viability to only 15%.

To further confirm these results, spheroids stained with calcein AM/PI were also imaged by CLSM (Figure 6). As expected, the nontreated spheroids and spheroids exposed solely to NIR light demonstrated an outer layer stained with calcein AM, indicating the presence of mostly viable cells, whereas the amount of PI-stained cells increased after PEtOx-IR/TOS NP incubation. The highest levels of PI staining were observed for spheroids treated with PEtOx-IR/TOS NPs plus NIR light.

Discussion

To address IR780's limitations (low water solubility and cytotoxicity), this NIR light-absorbing agent was conjugated with PEtOx-SH, with its successful synthesis confirmed by ^{1}H NMR and FTIR spectroscopy (Supplementary Figures 1 & 2). The resulting PEtOx-IR conjugate was then employed in the nanoprecipitation technique for assembling PEtOx-IR NPs (Figure 1A). This technique was selected because of its versatility, reproducibility and scalability [35,36]. Surprisingly, the hydrodynamic size of PEtOx-IR NPs (1092.0 ± 197.9 nm) (Figure 1B) was not within the optimal range for passive tumor accumulation (100–200 nm) [9,37]. The authors hypothesized that this could be due to subpar hydrophobic–hydrophobic interactions occurring in the particle core, which cannot drive the assembly of nanostructures.

To address this problem, TOS was also incorporated into the formulation because of its capacity to stabilize the nanomaterial core (yielding PEtOx-IR/TOS NPs). PEtOx-IR/TOS NPs had a size of 189.7 ± 4.4 nm (Figure 1B), which may enable their extravasation through the tumor's leaky vasculature – which demonstrates 200- to 1200-nm fenestrae – favoring their accumulation at the malignant site [38]. In a previous study, the incorporation of TOS in micelles formulated with PEGylated vitamin E also improved the size distribution [27]. The morphology of PEtOx-IR/TOS NPs (Supplementary Figure 3) was consistent with that of other IR780-based nanomaterials reported in the literature [39–45], which is appealing since spherically shaped nanostructures may display enhanced cellular uptake. Moreover, the surface charge of PEtOx-IR/TOS NPs (zeta potential: -7.8 ± 0.9 mV) was also within the range considered to be ideal for cancer-related applications (-10 to +10 mV) [29,46]. This feature may be attributed to the PEtOx-based corona of the nanostructures [20,47]. Equally significant is the so-called neutrally charged nanomaterials (-10 to +10 mV), which can display improved blood circulation time as a result of their weaker interaction with blood components, which favors tumor uptake [48–51]. The incorporation efficiency of the PEtOx-IR conjugate in PEtOx-IR/TOS NPs was also in line with that described for other IR780-based nanoformulations [9,52]. When PEtOx-IR/TOS NPs were dispersed in different media (water, PBS and DMEM-F12 supplemented with 10% [v/v] FBS), their size distribution and NIR absorption did not demonstrate meaningful variations over time (Supplementary Figure 4). This behavior may be attributed to the ability of the PEtOx-based coating to improve the colloidal stability of the nanostructures [18,20,53] and to the capacity of the TOS-hydrophobic core to protect the IR780 present in PEtOx-IR from degradation when dispersed in an aqueous medium [54,55].

PEtOx-IR/TOS NPs demonstrated the ability to interact with NIR light (Figure 1C), with an absorption at 808 nm that was 2.74- and 1.89-fold greater than that of the PEtOx-IR conjugate and PEtOx-IR NPs, respectively. This red shift in the absorption of PEtOx-IR/TOS NPs can be attributed to changes in solvent polarity and to hydrophobic–hydrophobic interactions occurring in the core of the NPs [27,54,56–58]. As a result, since 808-nm light is used in photothermal experiments, PEtOx-IR/TOS NPs may display a great photothermal capacity because of their higher absorption at 808 nm.

In photothermal capacity studies, PEtOx-IR/TOS NPs produced a temperature increase of 12.5°C after 2 min of exposure to NIR light, which can potentially cause cellular damage [4,32]. The highest photoinduced heat generated by PEtOx-IR/TOS NPs within the first 2 min of NIR laser exposure may be due to the photodegradation of IR780 by NIR light [9,11,59,60]. In fact, the optical properties of PEtOx-IR/TOS NPs in the NIR range were gradually lost after each minute of laser exposure (Supplementary Figure 7B). Because of this, PEtOx-IR/TOS NPs were not capable of producing a photothermal effect greater than that observed in the control after multiple NIR laser irradiation cycles (Supplementary Figure 7C). Nevertheless, this behavior displayed by PEtOx-IR/TOS NPs may be an important feature since the photodegradation products of IR780 were reported to be cytocompatible [13], hence possibly avoiding issues related to the long-term accumulation of photothermal nanoagents.

In the *in vitro* studies, PEtOx-IR NPs were shown to be cytocompatible in 2D cell cultures of NHDFs but capable to affect MCF-7 cell viability at high doses (7.5 and 10 μg ml^{-1} of PEtOx-IR conjugate equivalents) (Figure 2A & B). This cytotoxic profile in MCF-7 cells is likely due to the propensity of IR780 to accumulate in the mitochondria of these cells [61], which has also been reported for other IR780-based nanomedicines [27,55]. By contrast, NHDFs incubated with PEtOx-IR/TOS NPs did not demonstrate meaningful alterations in their viability at up to 5 μg ml^{-1} of PEtOx-IR conjugate equivalents (Figure 2C). MCF-7 cells incubated with PEtOx-IR/TOS NPs at this dose for 24 h also remained highly viable, but a longer incubation period (48 h) reduced their viability to 65% (Figure 2D). Greater doses of PEtOx-IR/TOS NPs (7.5 and 10 μg ml^{-1} of PEtOx-IR conjugate equivalents) induced high cytotoxicity in both NHDF and MCF-7 cells. Considering the behavior of PEtOx-IR NPs, the safety profile of PEtOx-IR/TOS NPs at high doses appears to be mainly influenced by TOS. In fact, TOS has

been reported to produce reactive oxygen species, which can affect both cell lines [62–66]. Because of this behavior, when assessing the internalization (4-h incubation period) and phototherapeutic capacity (24-h incubation period) of PEtOx-IR/TOS NPs in 2D *in vitro* cancer models, only doses of 2.5 and 5 μg ml^{-1} of PEtOx-IR conjugate equivalents were used to ensure that the observed effects were not masked by the action of TOS.

PEtOx-IR/TOS NPs were successfully internalized by monolayers of MCF-7 cells (Figure 3 & Supplementary Figure 8C). After subsequent NIR laser exposure (808 nm; 1.7 $W.cm^{-2}$; 5 min), PEtOx-IR/TOS NPs were able to decrease MCF-7 cell viability to just 9% at a very low dose (5 μg ml^{-1} of PEtOx-IR conjugate equivalents) (Figure 4B). Liu *et al.* produced IR780- and perfluoropentane-loaded PEGylated NPs (35.4 μg ml^{-1} of IR780 equivalents), revealing their ability to reduce B16 cell viability to about 55% upon NIR irradiation (808 nm; 2 $W.cm^{-2}$; 5 min) [67]. Song *et al.* produced IR780-loaded, folate-targeted NPs (40 μg ml^{-1}) that prompted a reduction in SKOV3 cell viability to 16% after NIR irradiation (808 nm; 1 $W.cm^{-2}$; 3 min) [68]. Shao *et al.* assembled RGD-functionalized, chitosan-based NPs encapsulating indocyanine green (40 μg ml^{-1}) that decreased SGC7901 cell viability to about 26% after NIR laser exposure (808 nm; 1 $W.cm^{-2}$; 5 min) [69]. Lima-Sousa *et al.* produced a PEtOx-coated, dopamine-reduced graphene oxide (75 μg ml^{-1}) that caused a reduction in MCF-7 cell viability to about 3% upon NIR laser irradiation (808 nm; 1.7 $W.cm^{-2}$; 5 min) [53]. Compared with these examples, the PTT mediated by PEtOx-IR/TOS NPs showed high efficacy at a lower dose of the photothermal agent, further corroborating the potential of this approach. Moreover, PEtOx-IR/TOS NPs mediated an on-demand effect in response to NIR light. This on-demand effect may be advantageous compared with strategies based on nanomaterials loaded with chemotherapy drugs since it carries a lower risk of off-target toxicity [4,70,71].

The performance of PEtOx-IR/TOS NPs was also screened using heterotypic breast cancer spheroids. This 3D *in vitro* cancer models was established using MCF-7 cells and NHDFs in order to mimic breast tumor cellular heterogeneity [72]. The 3D structure, cell–cell interactions and layered organization of spheroids grant them resistance to therapeutic penetration/action that is similar to that occurring in *in vivo* solid tumors [34,73]. Therefore, it is of the utmost importance to use spheroids in the screening of nanomaterial therapeutic capacity [33]. PEtOx-IR/TOS NPs were able to penetrate into spheroids but remained mostly at their periphery (Figure 5A). Such behavior results from the resistance of spheroids to penetration by nanomedicines and has been reported for other types of nanomaterials [30,74,75]. In addition, the combined action of PEtOx-IR/TOS NPs (15 μg ml^{-1} of PEtOx-IR conjugate equivalents) and NIR light (808 nm; 1.7 $W.cm^{-2}$; 5 min) decreased the viability of spheroids to 15% (Figure 5B). In a recent study, IR780- and doxorubicin-loaded sulfobetaine methacrylate-based NPs (9 μg ml^{-1} of IR780 equivalents and 6 μg ml^{-1} of doxorubicin) decreased heterotypic spheroid viability to 16% upon NIR laser irradiation (808 nm; 1.7 $W.cm^{-2}$; 5 min) [30]. In another study, IR780-loaded, PEG-based NPs functionalized with the CRGDK peptide (30 μg ml^{-1} of IR780 equivalents) decreased HT-29 spheroid viability to 54% after NIR laser exposure (808 nm, 2 $W.cm^{-2}$, 20 s) [75]. Gold–silica semishell NPs (60 μg ml^{-1}) were able to reduce U87-MG spheroid viability to 58% upon NIR laser irradiation (808 nm; 1.5 $W.cm^{-2}$; 7 min) [76]. The photothermal heating mediated by trimethyl chitosan-coated palladium NPs (220 μg ml^{-1}) decreased MDA-MB-231 spheroid viability to about 32% (808 nm; 1 $W.cm^{-2}$; 3 min) [77]. These examples demonstrate that PEtOx-IR/TOS NPs are promising agents for application in breast cancer PTT.

Conclusion

In this study, a PEtOx-IR conjugate was prepared for the first time and combined with TOS through the nanoprecipitation technique, leading to the assembly of PEtOx-IR/TOS NPs. PEtOx-IR/TOS NPs displayed suitable size (189.7 ± 4.4 nm) and surface charge (-7.8 ± 0.9 mV) for cancer-related applications. When incubated in different media, the size and NIR absorption of PEtOx-IR/TOS NPs did not show meaningful variations over time, suggesting that these nanostructures display good colloidal stability. By contrast, PEtOx-IR NPs (without TOS) did not exhibit suitable size distribution or proper stability. Moreover, PEtOx-IR/TOS NPs demonstrated 1.89- and 2.74-fold higher absorption at 808 nm than PEtOx-IR780 NPs and the PEtOx-IR conjugate, respectively, hence presenting greater photothermal potential. The *in vitro* assays suggested that PEtOx-IR/TOS NPs are cytocompatible with healthy cells at doses within the therapeutic range (up to 5 μg ml^{-1} of PEtOx-IR conjugate equivalents). When incubated in monolayers of cancer cells in 2D *in vitro* cancer cell models, PEtOx-IR/TOS NPs decreased cell viability to only 80%, whereas the combination of PEtOx-IR/TOS NPs and NIR light led to almost complete cancer cell ablation (viability <9%). The therapeutic potential of PEtOx-IR/TOS NPs was also screened in heterotypic spheroids (3D *in vitro* cancer cell models) and it was demonstrated the ability of PEtOx-IR/TOS

NPs to reduce spheroid viability to just 15% upon NIR laser irradiation. Overall, PEtOx-IR/TOS NPs appear to be promising agents for application in breast cancer PTT.

Future perspective

The inclusion of other agents (e.g., doxorubicin) in the core of PEtOx-IR/TOS NPs may further improve their therapeutic efficacy. In addition, *in vivo* assays will provide important insight into the biodistribution, biodegradability and tumor-ablating capability of this nanoformulation.

Summary points

- A novel poly(2-ethyl-2-oxazoline)–IR780 (PEtOx-IR) conjugate was prepared.
- A combination of PEtOx-IR and D-α-tocopheryl succinate (TOS) (PEtOx-IR/TOS) generated well-defined nanoparticles (NPs).
- PEtOx-IR/TOS NPs maintained their size distribution and near-infrared absorption when incubated in different media.
- PEtOx-IR/TOS NPs caused a temperature increase upon near-infrared laser exposure.
- PEtOx-IR/TOS NPs were successfully internalized by cancer cell monolayers (2D *in vitro* cancer models).
- The photothermal therapy mediated by PEtOx-IR/TOS NPs reduced the viability of breast cancer cells to 9%.
- PEtOx-IR/TOS NPs penetrated into heterotypic breast cancer spheroids (3D *in vitro* cancer models).
- The photothermal therapy mediated by PEtOx-IR/TOS NPs reduced spheroid viability to 15%.

Supplementary data

To view the supplementary data that accompany this paper please visit the journal website at: www.futuremedicine.com/doi/suppl/10.2217/nnm-2022-0218

Author contributions

Investigation, formal analysis and original draft: CG Alves. Investigation, review and editing: R Lima-Sousa. Investigation, review and editing: BL Melo. Investigation: P Ferreira. Investigation, review and editing: AF Moreira. Project administration, funding acquisition, supervision, review and editing: IJ Correia. Conceptualization, investigation, supervision, review and editing: D de Melo-Diogo.

Financial & competing interests disclosure

This study was developed within the scope of Centro de Investigação em Ciências da Saúde, Universidade da Beira Interior projects UIDB/00709/2020 and UIDP/00709/2020, financed by national funds through the Portuguese Foundation for Science and Technology/Ministry of Science, Technology and Higher Education. Funding from POCI-01-0145-FEDER-031462, PTDC/BTA-BTA/0696/2020 and 2022.06320.PTDC is also acknowledged. D de Melo-Diogo acknowledges the Foundation for Science and Technology for financial support given through a Junior Researcher contract (2021.00590.CEECIND). CG Alves, R Lima-Sousa and BL Melo acknowledge funding from individual PhD fellowships from the Foundation for Science and Technology (SFRH/BD/145386/2019, SFRH/BD/144922/2019 and 2021.06044.BD, respectively). The authors have no other relevant affiliations or financial involvement with any organization or entity with a financial interest in or financial conflict with the subject matter or materials discussed in the manuscript apart from those disclosed.

No writing assistance was utilized in the production of this manuscript.

References

Papers of special note have been highlighted as: • of interest; •• of considerable interest

1. Zhao L, Xing Y, Wang R, Yu F, Yu F. Self-assembled nanomaterials for enhanced phototherapy of cancer. *ACS Appl. Bio Mater.* 3(1), 86–106 (2019).
2. Li X, Zhong S, Zhang C, Li P, Ran H, Wang Z. MAGE-targeted gold nanoparticles for ultrasound imaging-guided phototherapy in melanoma. *Biomed Res. Int.* 2020, 6863231 (2020).
3. Curcio A, Silva AK, Cabana S *et al.* Iron oxide nanoflowers @ CuS hybrids for cancer tri-therapy: interplay of photothermal therapy, magnetic hyperthermia and photodynamic therapy. *Theranostics* 9(5), 1288 (2019).
4. Leitão MM, de Melo-Diogo D, Alves CG, Lima-Sousa R, Correia IJ. Prototypic heptamethine cyanine incorporating nanomaterials for cancer phototheragnostic. *Adv. Healthc. Mater.* 9(6), 1901665 (2020).

•• **Summarizes the potential of IR780 (IR)-based nanomaterials in cancer photothermal/photodynamic therapy.**

5. Vankayala R, Hwang KC. Near-infrared-light-activatable nanomaterial-mediated phototheranostic nanomedicines: an emerging paradigm for cancer treatment. *Adv. Mater.* 30(23), 1706320 (2018).
6. Wang H, Li X, Tse BW-C *et al.* Indocyanine green-incorporating nanoparticles for cancer theranostics. *Theranostics* 8(5), 1227 (2018).
7. Alves CG, Lima-Sousa R, Melo BL, Moreira AF, Correia IJ, de Melo-Diogo D. Heptamethine cyanine-loaded nanomaterials for cancer immuno-photothermal/photodynamic therapy: a review. *Pharmaceutics* 14(5), 1015 (2022).
8. Egloff-Juras C, Bezdetnaya L, Dolivet G, Lassalle H-P. NIR fluorescence-guided tumor surgery: new strategies for the use of indocyanine green. *Int. J. Nanomed.* 14, 7823 (2019).
9. Alves CG, de Melo-Diogo D, Lima-Sousa R, Costa EC, Correia IJ. Hyaluronic acid functionalized nanoparticles loaded with IR780 and DOX for cancer chemo-photothermal therapy. *Eur. J. Pharm. Biopharm.* 137, 86–94 (2019).

• **Explores the chemo-photothermal capacity of IR and doxorubicin-loaded nanoparticles (NPs).**

10. Lin T, Yuan A, Zhao X *et al.* Self-assembled tumor-targeting hyaluronic acid nanoparticles for photothermal ablation in orthotopic bladder cancer. *Acta Biomater.* 53(15), 427–438 (2017).
11. Qiu X, Xu L, Zhang Y *et al.* Photothermal ablation of *in situ* renal tumor by PEG-IR780-C13 micelles and near-infrared irradiation. *Mol. Pharm.* 13(3), 829–838 (2016).
12. de Oliveira MA, Machado MGC, Silva SED *et al.* IR780–polymer conjugates for stable near-infrared labeling of biodegradable polyester-based nanocarriers. *Eur. Polym. J.* 120, 109255 (2019).
13. Yuan A, Qiu X, Tang X, Liu W, Wu J, Hu Y. Self-assembled PEG-IR-780-C13 micelle as a targeting, safe and highly-effective photothermal agent for *in vivo* imaging and cancer therapy. *Biomaterials* 51, 184–193 (2015).
14. Wan G, Cheng Y, Song J *et al.* Nucleus-targeting near-infrared nanoparticles based on TAT peptide-conjugated IR780 for photo-chemotherapy of breast cancer. *Chem. Eng. J.* 380(15), 122458 (2020).
15. Nicolas J. Drug-initiated synthesis of polymer prodrugs: combining simplicity and efficacy in drug delivery. *Chem. Mater.* 28(6), 1591–1606 (2016).
16. Manandhar S, Sjöholm E, Bobacka J, Rosenholm JM, Bansal KK. Polymer–drug conjugates as nanotheranostic agents. *J. Nanotheranostics* 2(1), 63–81 (2021).
17. Ekladious I, Colson YL, Grinstaff MW. Polymer–drug conjugate therapeutics: advances, insights and prospects. *Nat. Rev. Drug Discov.* 18(4), 273–294 (2019).
18. Novy Z, Lobaz V, Vlk M *et al.* Head-to-head comparison of biological behavior of biocompatible polymers poly (ethylene oxide), poly (2-ethyl-2-oxazoline) and poly [*N*-(2-hydroxypropyl) methacrylamide] as coating materials for hydroxyapatite nanoparticles in animal solid tumor model. *Nanomaterials (Basel)* 10(9), 1690 (2020).

•• **Reports the *in vivo* behavior of NPs coated with poly(2-ethyl-2-oxazoline).**

19. Bludau H, Czapar AE, Pitek AS, Shukla S, Jordan R, Steinmetz NF. POxylation as an alternative stealth coating for biomedical applications. *Eur. Polym. J.* 88, 679–688 (2017).
20. Koshkina O, Westmeier D, Lang T *et al.* Tuning the surface of nanoparticles: impact of poly (2-ethyl-2-oxazoline) on protein adsorption in serum and cellular uptake. *Macromol. Biosci.* 16(9), 1287–1300 (2016).
21. Fam SY, Chee CF, Yong CY, Ho KL, Mariatulqabtiah AR, Tan WS. Stealth coating of nanoparticles in drug-delivery systems. *Nanomaterials (Basel)* 10(4), 787 (2020).
22. Xu H, Zhang W, Li Y *et al.* The bifunctional liposomes constructed by poly(2-ethyl-oxazoline)-cholesteryl methyl carbonate: an effectual approach to enhance liposomal circulation time, pH-sensitivity and endosomal escape. *Pharm. Res.* 31(11), 3038–3050 (2014).
23. Gao N, Xing C, Wang H *et al.* pH-responsive dual drug-loaded nanocarriers based on poly (2-ethyl-2-oxazoline) modified black phosphorus nanosheets for cancer chemo/photothermal therapy. *Front. Pharmacol.* 10, 270 (2019).
24. Abu Lila AS, Kiwada H, Ishida T. The accelerated blood clearance (ABC) phenomenon: clinical challenge and approaches to manage. *J. Control. Rel.* 172(1), 38–47 (2013).
25. d'Avanzo N, Celia C, Barone A *et al.* Immunogenicity of polyethylene glycol based nanomedicines: mechanisms, clinical implications and systematic approach. *Adv. Ther.* 3(3), 1900170 (2020).
26. Luo N, Weber JK, Wang S *et al.* PEGylated graphene oxide elicits strong immunological responses despite surface passivation. *Nat. Commun.* 8(1), 1–10 (2017).
27. Pais-Silva C, de Melo-Diogo D, Correia IJ. IR780-loaded TPGS-TOS micelles for breast cancer photodynamic therapy. *Eur. J. Pharm. Biopharm.* 113, 108–117 (2017).

• **Analyzes the effect of D-α-tocopheryl succinate (TOS) in the assembly of IR-incorporating nanomaterials.**

28. Tsai M-H, Peng C-L, Yang S-J, Shieh M-J. Photothermal, targeting, theranostic near-infrared nanoagent with SN38 against colorectal cancer for chemothermal therapy. *Mol. Pharm.* 14(8), 2766–2780 (2017).
29. Alves CG, de Melo-Diogo D, Lima-Sousa R, Correia IJ. IR780 loaded sulfobetaine methacrylate-functionalized albumin nanoparticles aimed for enhanced breast cancer phototherapy. *Int. J. Pharm.* 582(30), 119346 (2020).

30. Mó I, Alves CG, de Melo-Diogo D, Lima-Sousa R, Correia IJ. Assessing the combinatorial chemo-photothermal therapy mediated by sulfobetaine methacrylate-functionalized nanoparticles in 2D and 3D *in vitro* cancer models. *Biotechnol. J.* 15(12), 2000219 (2020).
31. Lima-Sousa R, de Melo-Diogo D, Alves CG *et al.* Hyaluronic acid functionalized green reduced graphene oxide for targeted cancer photothermal therapy. *Carbohydr. Polym.* 200, 93–99 (2018).
32. de Melo-Diogo D, Lima-Sousa R, Alves CG, Correia IJ. Graphene family nanomaterials for application in cancer combination photothermal therapy. *Biomater. Sci.* 7(9), 3534–3551 (2019).
33. Mó I, Sabino IJ, de Melo-Diogo D, Lima-Sousa R, Alves CG, Correia IJ. The importance of spheroids in analyzing nanomedicine efficacy. *Nanomedicine (Lond.)* 15(15), 1513–1525 (2020).
34. Lu H, Stenzel MH. Multicellular tumor spheroids (MCTS) as a 3D *in vitro* evaluation tool of nanoparticles. *Small* 14(13), 1702858 (2018).
35. Barreras-Urbina CG, Ramírez-Wong B, López-Ahumada GA *et al.* Nano- and micro-particles by nanoprecipitation: possible application in the food and agricultural industries. *Int. J. Food Prop.* 19(9), 1912–1923 (2016).
36. Martínez Rivas CJ, Tarhini M, Badri W *et al.* Nanoprecipitation process: from encapsulation to drug delivery. *Int. J. Pharm.* 532(1), 66–81 (2017).
37. Blanco E, Shen H, Ferrari M. Principles of nanoparticle design for overcoming biological barriers to drug delivery. *Nat. Biotechnol.* 33(9), 941 (2015).
38. Vu-Quang H, Vinding MS, Nielsen T *et al.* Pluronic F127–folate coated super paramagenic iron oxide nanoparticles as contrast agent for cancer diagnosis in magnetic resonance imaging. *Polymers (Basel)* 11(4), 743 (2019).
39. Chen M, Bhattarai N, Cong M, Pérez RL, McDonough KC, Warner IM. Mitochondria targeting IR780-based nanoGUMBOS for enhanced selective toxicity towards cancer cells. *RSC Adv.* 8(55), 31700–31709 (2018).
40. Tan Y, Zhu Y, Wen L *et al.* Mitochondria-responsive drug release along with heat shock mediated by multifunctional glycolipid micelles for precise cancer chemo-phototherapy. *Theranostics* 9(3), 691–707 (2019).
41. Li Y, Kröger M, Liu WK. Shape effect in cellular uptake of PEGylated nanoparticles: comparison between sphere, rod, cube and disk. *Nanoscale* 7(40), 16631–16646 (2015).
42. Dias DR, Moreira AF, Correia IJ. The effect of the shape of gold core–mesoporous silica shell nanoparticles on the cellular behavior and tumor spheroid penetration. *J. Mater. Chem. B* 4(47), 7630–7640 (2016).
43. Chithrani DB. Intracellular uptake, transport, and processing of gold nanostructures. *Mol. Membr. Biol.* 27(7), 299–311 (2010).
44. Zhang K, Fang H, Chen Z, Taylor J-SA, Wooley KL. Shape effects of nanoparticles conjugated with cell-penetrating peptides (HIV Tat PTD) on CHO cell uptake. *Bioconjug. Chem.* 19(9), 1880–1887 (2008).
45. Zhao J, Lu H, Wong S, Lu M, Xiao P, Stenzel MH. Influence of nanoparticle shapes on cellular uptake of paclitaxel loaded nanoparticles in 2D and 3D cancer models. *Polym. Chem.* 8(21), 3317–3326 (2017).
46. Ernsting MJ, Murakami M, Roy A, Li S-D. Factors controlling the pharmacokinetics, biodistribution and intratumoral penetration of nanoparticles. *J. Control. Rel.* 172(3), 782–794 (2013).
47. Hsiue G-H, Wang C-H, Lo C-L, Wang C-H, Li J-P, Yang J-L. Environmental-sensitive micelles based on poly (2-ethyl-2-oxazoline)-b-poly (L-lactide) diblock copolymer for application in drug delivery. *Int. J. Pharm.* 317(1), 69–75 (2006).
48. Yang G, Xu L, Xu J *et al.* Smart nanoreactors for pH-responsive tumor homing, mitochondria-targeting, and enhanced photodynamic-immunotherapy of cancer. *Nano Lett.* 18(4), 2475–2484 (2018).
49. de Melo-Diogo D, Pais-Silva C, Dias DR, Moreira AF, Correia IJ. Strategies to improve cancer photothermal therapy mediated by nanomaterials. *Adv. Healthc. Mater.* 6(10), 1700073 (2017).
50. Dai L, Li K, Li M *et al.* Size/charge changeable acidity-responsive micelleplex for photodynamic-improved PD-L1 immunotherapy with enhanced tumor penetration. *Adv. Funct. Mater.* 28(18), 1707249 (2018).
51. Duan X, Li Y. Physicochemical characteristics of nanoparticles affect circulation, biodistribution, cellular internalization, and trafficking. *Small* 9(9–10), 1521–1532 (2013).
52. Kulbacka J, Pucek A, Kotulska M *et al.* Electroporation and lipid nanoparticles with cyanine IR-780 and flavonoids as efficient vectors to enhanced drug delivery in colon cancer. *Bioelectrochemistry* 110, 19–31 (2016).
53. Lima-Sousa R, Alves CG, Melo BL *et al.* Poly(2-ethyl-2-oxazoline) functionalized reduced graphene oxide: optimization of the reduction process using dopamine and application in cancer photothermal therapy. *Mater. Sci. Eng. C Mater. Biol. Appl.* 130, 112468 (2021).
54. Wang K, Zhang Y, Wang J *et al.* Self-assembled IR780-loaded transferrin nanoparticles as an imaging, targeting and PDT/PTT agent for cancer therapy. *Sci. Rep.* 6(1), 1–11 (2016).
55. Jiang C, Cheng H, Yuan A, Tang X, Wu J, Hu Y. Hydrophobic IR780 encapsulated in biodegradable human serum albumin nanoparticles for photothermal and photodynamic therapy. *Acta Biomater.* 14(1), 61–69 (2015).
56. Kuang Y, Zhang K, Cao Y *et al.* Hydrophobic IR-780 dye encapsulated in cRGD-conjugated solid lipid nanoparticles for NIR imaging-guided photothermal therapy. *ACS Appl. Mater. Interfaces* 9(14), 12217–12226 (2017).

57. Potara M, Nagy-Simon T, Focsan M *et al.* Folate-targeted pluronic–chitosan nanocapsules loaded with IR780 for near-infrared fluorescence imaging and photothermal–photodynamic therapy of ovarian cancer. *Colloids Surf. B Biointerfaces* 203, 111755 (2021).
58. Liu G, Lin T, Zhang Q *et al.* Hyaluronic acid–IR780 nanoparticles for photothermal ablation in orthotopic renal cancer. *J. Nanomater.* 2020, 2421971 (2020).
59. Chen Y, Li Z, Wang H *et al.* IR-780 loaded phospholipid mimicking homopolymeric micelles for near-IR imaging and photothermal therapy of pancreatic cancer. *ACS Appl. Mater. Interfaces* 8(11), 6852–6858 (2016).
60. Guo F, Yu M, Wang J, Tan F, Li N. The mitochondria-targeted and IR780-regulated theranosomes for imaging and enhanced photodynamic/photothermal therapy. *RSC Adv.* 6(14), 11070–11076 (2016).
61. Zhang C, Liu T, Su Y *et al.* A near-infrared fluorescent heptamethine indocyanine dye with preferential tumor accumulation for *in vivo* imaging. *Biomaterials* 31(25), 6612–6617 (2010).
62. Duhem N, Danhier F, Préat V. Vitamin E-based nanomedicines for anti-cancer drug delivery. *J. Control. Rel.* 182, 33–44 (2014).
63. Constantinou C, Papas A, Constantinou AI. Vitamin E and cancer: an insight into the anticancer activities of vitamin E isomers and analogs. *Int. J. Cancer* 123(4), 739–752 (2008).
64. Meyenberg A, Goldblum D, Zingg J-M *et al.* Tocotrienol inhibits proliferation of human Tenon's fibroblasts *in vitro*: a comparative study with vitamin E forms and mitomycin C. *Graefes Arch. Clin. Exp. Ophthalmol.* 243(12), 1263–1271 (2005).
65. Gupta AK, Wells S. Surface-modified superparamagnetic nanoparticles for drug delivery: preparation, characterization, and cytotoxicity studies. *IEEE Trans. Nanobiosci.* 3(1), 66–73 (2004).
66. Danhier F, Kouhé TTB, Duhem N *et al.* Vitamin E-based micelles enhance the anticancer activity of doxorubicin. *Int. J. Pharm.* 476(1–2), 9–15 (2014).
67. Liu M, Zhang P, Deng L *et al.* IR780-based light-responsive nanocomplexes combining phase transition for enhancing multimodal imaging-guided photothermal therapy. *Biomater. Sci.* 7(3), 1132–1146 (2019).
68. Song J, Zhang N, Zhang L *et al.* IR780-loaded folate-targeted nanoparticles for near-infrared fluorescence image-guided surgery and photothermal therapy in ovarian cancer. *Int. J. Nanomed.* 14, 2757 (2019).
69. Shao J, Liang R, Ding D *et al.* A smart multifunctional nanoparticle for enhanced near-infrared image-guided photothermal therapy against gastric cancer. *Int. J. Nanomed.* 16, 2897–2915 (2021).
70. Wang X, Xuan Z, Zhu X, Sun H, Li J, Xie Z. Near-infrared photoresponsive drug delivery nanosystems for cancer photo-chemotherapy. *J. Nanobiotechnol.* 18(1), 108 (2020).
71. Li J, Pu K. Semiconducting polymer nanomaterials as near-infrared photoactivatable protherapeutics for cancer. *Acc. Chem. Res.* 53(4), 752–762 (2020).
72. Zanoni M, Piccinini F, Arienti C *et al.* 3D tumor spheroid models for *in vitro* therapeutic screening: a systematic approach to enhance the biological relevance of data obtained. *Sci. Rep.* 6(1), 1–11 (2016).
73. Mehta G, Hsiao AY, Ingram M, Luker GD, Takayama S. Opportunities and challenges for use of tumor spheroids as models to test drug delivery and efficacy. *J. Control. Rel.* 164(2), 192–204 (2012).
74. Wang X, Zhen X, Wang J, Zhang J, Wu W, Jiang X. Doxorubicin delivery to 3D multicellular spheroids and tumors based on boronic acid-rich chitosan nanoparticles. *Biomaterials* 34(19), 4667–4679 (2013).
75. Zhao C, Tong Y, Li X *et al.* Photosensitive nanoparticles combining vascular-independent intratumor distribution and on-demand oxygen-depot delivery for enhanced cancer photodynamic therapy. *Small* 14(12), 1703045 (2018).
76. Li W, Ma J, Garcia S *et al.* Semishell Janus nanoparticle-enabled pH-responsive rod-shaped assembly for photothermal therapy. *ACS Appl. Nano Mater.* 5(1), 871–880 (2022).
77. Bangde P, Pant T, Gaikwad G, Jain R, Dandekar P. Trimethyl chitosan coated palladium nanoparticles as a photothermal agent and its *in vitro* evaluation in 2D and 3D model of breast cancer cells. *Colloids Surf. B Biointerfaces* 211, 112287 (2022).